

Small bipolarons and extended states of guest Na and Rb atoms in quasi-two-dimensional disordered $M_{7.8-\delta}Al_{7.8}Si_{8.2}O_{32.0}$ ($M=Na, Rb$)

Gayan Prasad Hettiarachchi,^{1,2,*} Fumiya Moriasa,² Yoshihumi Nishida,² Takehito Nakano,² Mohd Nazlan Mohd Muhid,³ and Halimaton Hamdan³

¹*Institute for NanoScience Design, Osaka University, Osaka 560-8531, Japan*

²*Department of Physics, Graduate School of Science, Osaka University, Osaka 560-0043, Japan*

³*Department of Chemistry, Faculty of Science, University of Technology Malaysia, 81310 Skudai, Johor, Malaysia*

(Received 26 January 2017; revised manuscript received 14 July 2017; published 12 October 2017)

The evolution of the electronic properties of guest Na and Rb atoms in a disordered deformable lattice is investigated for a series of guest-atom densities n . The quasi-two-dimensional host $M_{7.8-\delta}Al_{7.8}Si_{8.2}O_{32.0}$ ($M=Na, Rb$), known as zeolite P, is used. The Na system is a stubborn bipolaronic insulator to the maximum n of 1.03. In contrast, the Rb system exhibits a crossover from a bipolaronic insulator to a conducting phase analogous to a disordered metal at $n = 0.89$. A critical region undergoing polaronic melting appears in the vicinity of the crossover on the insulating side, evidenced by a reduction in the small bipolaron absorption band and a drop in the activation energy. Transition to the conducting phase coincides with the appearance of a midinfrared band and an increase in the charge-carrier decay length, suggesting the polaronic and extended nature of the carriers. These findings constitute rare examples of electron-lattice coupling opening (or closing) a mobility gap and scaling the continuity (or discontinuity) of a conducting transition in the face of disorder.

DOI: [10.1103/PhysRevB.96.155115](https://doi.org/10.1103/PhysRevB.96.155115)

I. INTRODUCTION

In 1933, Landau introduced the concept of a polaron, the stable ground state of an electron in a polarizable ionic lattice, where the electron self-traps as a result of a simultaneous lattice deformation [1]. The polaron is characterized by its binding energy and effective mass [2,3], and its properties differ from those of a band electron. Polaronic effects are thought to play important roles in high-transition-temperature (T_c) superconductivity [4–6], magnetism in magnetic semiconductors [7,8], manganites [4,9], and metal clusters in zeolites [10], along with transport in organic materials [11,12], transition-metal oxides [13], alkali-doped zeolites [10,14,15], and conjugated polymers [16,17]. The two general limits of the polaron distinguish small (Holstein) [18,19] and large (Frölich) polarons [3,4]. Small polarons are localized at temperature $T = 0$ K with large binding energy and heavy mass [20], whereas large polarons are extended and exhibit finite electrostatic interaction with the lattice [3,4,21]. The relevant energy scales at which these quasiparticles form (or collapse) are difficult to predict. Further, their correlations, dynamics, and transport in a many-polaron system are nontrivial.

Polaronic effects are particularly strong in disordered systems, as slow diffusion or localization promotes local lattice deformations [22]. The nontrivial interplay of disorder and the correlated response of a deformable lattice to the random potential render the electron-lattice coupling strength λ a vital parameter near the mobility edge. The scaling theory of localization in disordered media [23,24] which provides an extension to the Anderson transition [25] by including electron correlations, yields a generic picture of a continuous conducting transition. Despite the use of the density of states (DOS) in the renormalization group, this model has been proven useful for explaining experimental results [24,26,27].

By combining the scaling theory of localization in disordered media [23,24] with the Emin and Holstein scaling theory for polaron formation [28], Cohen *et al.* [29,30] have suggested a discontinuous transition between extended and self-trapped states, with the discontinuity being proportional to $\lambda^{2/3}$.

Theoretical treatment of the metal-insulator transition (MIT) in a deformable lattice, which attached equal weight to Anderson localization and polaronic effects due to electron-lattice coupling [31], has highlighted the opening of a mobility gap in the strong-coupling regime; the gap remains open even in the case of weak disorder in the random potential. For weaker coupling, varying the disorder in the random potential from strong to weak yields a continuous MIT. The conducting phase is characterized by the appearance of extended states followed by conventional metallic states [31]. It is suggested that the extended states, analogous to a disordered metal [32,33], exhibit a negative temperature coefficient of resistivity (TCR) [31] with finite conductivity σ at $T = 0$. However, despite a considerable body of theoretical study addressing the issue of electron-lattice coupling near the mobility edge, experimental investigations are scarce or even nonexistent, to the best of our knowledge.

In this study, we experimentally investigate the properties of electrons in a disordered deformable lattice, controlling the random potential through electron-density modulation. We use the quasi-two-dimensional (quasi-2D) host $M_{7.8-\delta}Al_{7.8}Si_{8.2}O_{32.0}$, known as zeolite P, which contains a cationic deformable lattice ($M=Na$ or Rb) within the negatively charged aluminosilicate framework ($Al_{7.8}Si_{8.2}O_{32.0}$). We introduce guest Na or Rb atoms to modulate the electron density and, in turn, the random potential. The interactions between the guest s electrons and the deformable lattice induce the electron-lattice coupling [10,14]. We report on the Na system, which remains a bipolaronic insulator by maintaining a mobility gap even at high electron density (i.e., weak disorder in the random potential), and on the crossover of the Rb system from small bipolarons to extended states,

*hettiarachchi@hpr.stec.es.osaka-u.ac.jp

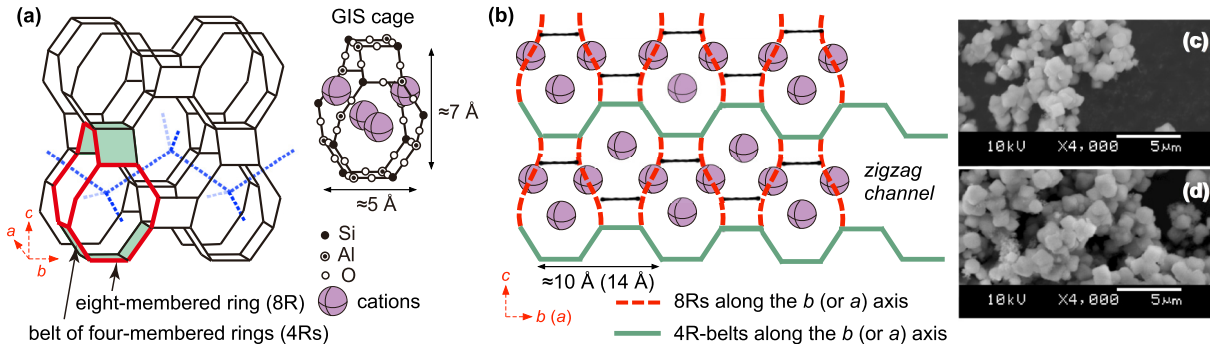


FIG. 1. The structure of the host material. (a) Aluminosilicate framework of zeolite P. The constructing element, the GIS cage with Si/Al = 1, is illustrated on the right-hand side. The purple spheres represent the cations (Na or Rb) that form the deformable lattice. The blue dotted lines represent the connections between cage voids of adjacent channels forming a diamond lattice. (b) Channel view along the *b* (or *a*) axis. SEM images of (c) Na-form and (d) Rb-form zeolite P.

which are in agreement with a recent theoretical investigation [31]. We note that this does not exclude the suggested discontinuous transition [29,30]. The conducting transition of K atoms in the same system [15] is in agreement with the proposed discontinuity [29]. We highlight the importance of the magnitude of λ on the conducting transition and its continuity (or discontinuity) when the nontrivial interplay of disorder and the correlated response of the lattice to the random potential cannot be disregarded. We conjecture that both theories [29,31] apply, perhaps in two distinct coupling regimes.

II. EXPERIMENT

We used powder samples of Na-form zeolite P [34] as the starting material. The framework of zeolite P is shown in Fig. 1(a) and comprises a periodic arrangement of gismondine (GIS) cages. One such GIS cage is illustrated on the right-hand side of Fig. 1(a). When the Si-to-Al ratio (Si/Al) is 1, the Si and Al atoms are alternately ordered [35]. The GIS cage comprises four eight-membered rings (8Rs) and six four-membered rings (4Rs). The cations are located near the centers of the 8Rs [36]. The four 8Rs are shared between cages, forming zigzag channels along the *a* and *b* axes [Fig. 1(b)]. Perpendicular connections of these zigzag channels form a quasi-2D structure. The green shaded areas in Fig. 1(a) show belts formed by the three 4Rs at the top and bottom of the highlighted cage. The continuous connections of these belts along the *a* and *b* axes [Fig. 1(b)] yield a 2D slab in the *ab* plane. The cage voids across adjacent channels can be connected in a diamond lattice, as illustrated by the blue dotted lines in Fig. 1(a).

Images of Na-form and Rb-form zeolite P obtained using a Joel JSM-6060LV scanning electron microscope (SEM) operating at 10 kV are shown in Figs. 1(c) and 1(d), respectively. The average crystal size is $\approx 1 \mu\text{m}$. The chemical formula per GIS cage of Na-form zeolite P estimated based on inductively coupled plasma optical emission spectrometry is $\text{Na}_{1.85}\text{Al}_{1.95}\text{Si}_{2.05}\text{O}_{8.00}$ ($\text{Na}_2\text{-P}$). Note that the unit cell comprises four GIS cages. Rb-form zeolite P was obtained through ionic exchange of K-form zeolite P (itself obtained through ionic exchange of Na-form zeolite P in a KCl aqueous solution) in a RbCl aqueous solution. The estimated chemical formula of Rb-form zeolite P per GIS cage is

$\text{Rb}_{1.90}\text{Al}_{1.95}\text{Si}_{2.05}\text{O}_{8.00}$ ($\text{Rb}_2\text{-P}$). When Si/Al > 1 (being 1.05 in both cases), the presence of -Si-O-Si- bonds yields weak disorder in the cation distribution. The deficiency in *M* suggests that a small number of cations are exchanged for protons, adding to the disorder. In this study, the average guest-atom density per GIS cage is defined as *n*, and the chemical formulas are rewritten as $\text{Na}_{1.85+n}\text{Al}_{1.95}\text{Si}_{2.05}\text{O}_{8.00}$ and $\text{Rb}_{1.90+n}\text{Al}_{1.95}\text{Si}_{2.05}\text{O}_{8.00}$, abbreviated as $\text{Na}_n/\text{Na}_2\text{-P}$ and $\text{Rb}_n/\text{Rb}_2\text{-P}$, respectively. To facilitate comparison of these systems with the previously reported K system mentioned above [15], the notation $\text{K}_n/\text{K}_2\text{-P}$ is used. Samples of $\text{Na}_n/\text{Na}_2\text{-P}$ ($n = 0.05, 0.16, 0.29, 0.41, 0.52, 0.62, 0.71, 0.83, 0.89,$ and 1.03) and $\text{Rb}_n/\text{Rb}_2\text{-P}$ ($n = 0.12, 0.21, 0.29, 0.40, 0.52, 0.61, 0.70, 0.81, 0.89,$ and 0.99) were synthesized through vapor adsorption of accurately weighed Na (Rb) metal into $\text{Na}_2\text{-P}$ ($\text{Rb}_2\text{-P}$) at 150 °C (100 °C) inside sealed glass tubes.

Optical, magnetic, and transport measurements were performed on all samples. The diffuse reflectance $r(\omega)$ of the powder samples was measured at room temperature using an ultraviolet-visible-near-infrared spectrometer (Cary 5G, Varian) and a Fourier transform infrared spectrometer (Nicolet MAGNA 550). The optical absorption was obtained using the Kubelka-Munk transformation $k/s = (1 - r)^2/2r$ [37], where *k* and *s* are the absorption and scattering coefficients, respectively. Direct-current electrical resistivity ρ measurements of pressed powder samples were performed using a physical property measurement system (PPMS, Quantum Design) in the *T* range 10–300 K. The dc magnetization was measured using a superconducting quantum interference device magnetometer (Quantum Design MPMS-XL) in the *T* range 1.8–300 K. All measurements were performed on samples sealed inside glass tubes, except for the ρ measurements, for which the measurement setup was sealed inside an airproof cell.

III. RESULTS

The optical absorption spectra of $\text{Na}_n/\text{Na}_2\text{-P}$ at $n = 0.05, 0.29, 0.41, 0.62, 0.71, 0.83,$ and 1.03 are shown in Fig. 2(a). At $n = 0.05$, an absorption band appears at approximately $21\,000 \text{ cm}^{-1}$ [solid circles, Fig. 2(a)] and is superimposed on a band in the UV region. The band in the UV region, which is

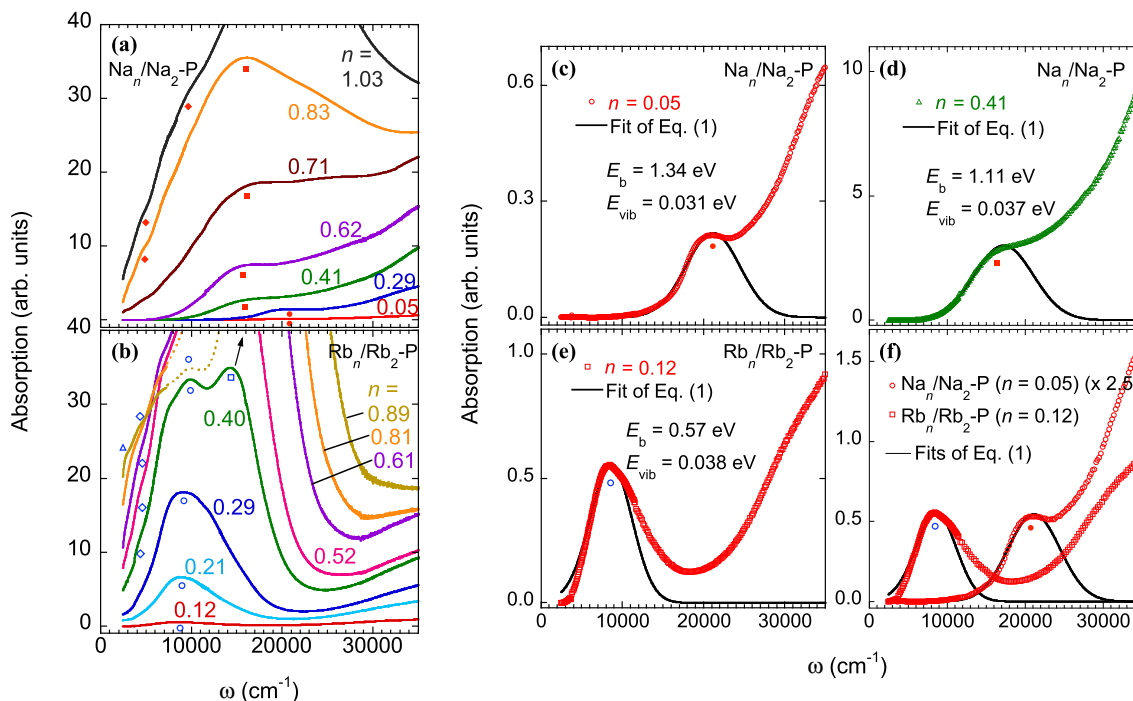


FIG. 2. Room-temperature optical absorption spectra of (a) $\text{Na}_n/\text{Na}_2\text{-P}$ and (b) $\text{Rb}_n/\text{Rb}_2\text{-P}$. The dotted lines in (b) starting at $n = 0.81$ indicate reduction in the band at approximately 8500 cm^{-1} . Best fits of small-polaron absorption [Eq. (1)] on $\text{Na}_n/\text{Na}_2\text{-P}$ (c) at $n = 0.05$ and (d) at $n = 0.41$ and on $\text{Rb}_n/\text{Rb}_2\text{-P}$ (e) at $n = 0.12$. (f) Absorption bands of $\text{Na}_n/\text{Na}_2\text{-P}$ and $\text{Rb}_n/\text{Rb}_2\text{-P}$ at the lowest values of n .

also observed in other zeolite materials is assigned to charge-transfer excitations in the aluminosilicate framework [38], and is outside the main interest of this study. A small (bi)polaron can form when short-range electron-lattice coupling, such as the deformation-potential interaction, is dominant [39,40]. This behavior becomes prevalent in the presence of a deformable ionic lattice, which induces Frank-Condon displacements and self-trapping. The optical absorptions carry vital information pertaining to these self-trapped states.

The optical excitations of small (bi)polarons produce quite characteristic absorption(s) in the visible and/or midinfrared (MIR) region(s) [39–42]. A small polaron exhibits an asymmetric absorption at the resonant excitation energy $\hbar\omega = 2E_b$ [40], where E_b is the small-polaron binding energy, \hbar is the reduced Planck constant, and ω is the angular frequency. For an intrasite small bipolaron (i.e., two trapped carriers occupying the same site), the absorption energy is $4E_b - U$ [40], where U is the on-site Coulomb repulsion energy. The small-polaron absorption spectrum $\alpha_{\text{sp}}(\omega)$ proposed by Emin [40] is given by

$$\alpha_{\text{sp}}(\omega) = \frac{2(\pi)^{3/2}e^2}{m^*c} \frac{t'}{(8E_b E_{\text{vib}})^{1/2}} \exp\left[-\frac{(2E_b - \hbar\omega)^2}{8E_b E_{\text{vib}}}\right], \quad (1)$$

where m^* is the effective electronic mass, c is the speed of light, t' ($\equiv \hbar^2/2m^*a^2$) is the intersite electronic transfer energy, a is a lattice constant, and E_{vib} is the characteristic vibrational energy. The $\alpha_{\text{sp}}(\omega)$ term gives the absorption coefficient per unit small-polaron density. The formation of small bipolarons is proposed in Sec. IV; however, for simplicity and because of the unavailability of direct experimental evidence indicating whether the small bipolarons are intra- [43] or intersite [6], we use the $\alpha_{\text{sp}}(\omega)$ given in Eq. (1)

when fitting the absorption spectra. (Note that the intersite scenario is most plausible for small bipolarons proposed in this study, i.e., a weakly paired state of two small polarons [43].) This produces an ambiguity in the estimated E_b by a factor of 2 (depending on whether $\hbar\omega = 2E_b$ or $\approx 4E_b$). However, this does not hinder comparisons of the relative strength of E_b between systems with comparable ground states.

The best fit of $\alpha_{\text{sp}}(\omega)$ with $E_b = 1.34 \text{ eV}$ on the band around 21000 cm^{-1} at $n = 0.05$ is shown in Fig. 2(c). This band grows with increasing n to $n = 0.29$. At $n = 0.41$, the band around 21000 cm^{-1} decreases, and a new band appears at a lower frequency at approximately 16000 cm^{-1} [solid squares, Fig. 2(a)]. The best fit of $\alpha_{\text{sp}}(\omega)$ for $n = 0.41$ with $E_b = 1.11 \text{ eV}$ is shown in Fig. 2(d). This broad band at approximately 16000 cm^{-1} grows with increasing n . Several shoulders appear in the tail at high n (≥ 0.83), which are marked by solid diamonds in Fig. 2(a). The exponentially decreasing absorption tails for $n \leq 0.62$ indicate a finite optical gap. With a further increase in n (> 0.71), the tail extends to lower frequencies, suggesting a decrease in the gap.

The room-temperature optical absorption spectra of $\text{Rb}_n/\text{Rb}_2\text{-P}$ at $n = 0.12, 0.21, 0.29, 0.40, 0.52, 0.61, 0.81,$ and 0.89 are shown in Fig. 2(b). At $n = 0.12$, an absorption band appears at approximately 8500 cm^{-1} [open circles, Fig. 2(b)] and is superimposed onto a band in the UV region [38]. The best fit of $\alpha_{\text{sp}}(\omega)$ for $n = 0.12$ with $E_b = 0.57 \text{ eV}$ is shown in Fig. 2(e). The fitting parameters of the curves shown in Figs. 2(c)–(e) are summarized in Table I. At $n = 0.40$, new bands appear at approximately 14500 cm^{-1} [open square, Fig. 2(b)] and 3300 cm^{-1} in the MIR [open diamonds, Fig. 2(b)]. These bands coexist with that at 8500 cm^{-1} . With increasing n , the band in the vicinity of 14500 cm^{-1} grows

with a blueshift, whereas that at approximately 8500 cm^{-1} grows ($n < 0.81$) at fixed energy. This behavior is different from that of $\text{Na}_n/\text{Na}_2\text{-P}$, where the band at approximately $21\,000\text{ cm}^{-1}$ is suppressed upon the appearance of the new band at approximately $16\,000\text{ cm}^{-1}$. Even though $n \approx 0.4$ marks a key density at which a notable change occurs, the subsequent behavior differs between $\text{Na}_n/\text{Na}_2\text{-P}$ and $\text{Rb}_n/\text{Rb}_2\text{-P}$. Starting at $n = 0.81$, the band at approximately 8500 cm^{-1} exhibits a continuous reduction [the spectral area indicated by the dotted lines in Fig. 2(b)], but remains intact to the maximum n of 0.99. Following this reduction, a second MIR band appears at approximately 2500 cm^{-1} at $n = 0.89$ [open triangle, Fig. 2(b)]. The absorption tail suggests a finite optical gap at $n = 0.12$ and a decrease in the gap with increasing n .

The ρ of $\text{Na}_n/\text{Na}_2\text{-P}$ for $n \leq 0.89$ is very high ($> 10^9\ \Omega\text{ cm}$; the noise limit of the measurement) from 300 down to 10 K, which is the lowest measurement T employed in this study. At $n = 1.03$, $\rho \approx 4 \times 10^8\ \Omega\text{ cm}$ at 300 K [Fig. 3(b)] but exceeds $10^9\ \Omega\text{ cm}$ at approximately 260 K, increasing with decreasing T . Thus, the $\text{Na}_n/\text{Na}_2\text{-P}$ samples are insulating despite the possible decrease in the optical gap. Note that the ρ of a single particle cannot be observed because of the granular nature of the samples, but the measurements enable granular comparisons between samples. The result reproducibility was confirmed through several runs with different samples having the same (or comparable) values of n .

The T dependence of ρ pertaining to $\text{Rb}_n/\text{Rb}_2\text{-P}$ is shown in Fig. 3(a) for $0.40 \leq n \leq 0.99$ in the cooling process from 300 to 10 K. The $\text{Rb}_n/\text{Rb}_2\text{-P}$ samples are insulating for $n \leq 0.81$. Beginning at $n = 0.89$, very low ρ is observed at 10 K. However, in contrast to a conventional metal, a negative TCR is observed. At low T ($< 100\text{ K}$), σ for $n = 0.89$ and 0.99 exhibits $T^{\frac{1}{2}}$ behavior with the form $\sigma = \sigma_0 + \sigma_1 T^{\frac{1}{2}}$ (not shown here; σ_0 represents σ at $T = 0$ and σ_1 is a constant), which is characteristic of diffusive (extended) transport in disordered metals with enhanced electron-electron interactions and weak localization effects [24,26,27,33,44–46]. Further, σ_0 is finite for $n = 0.89$ and 0.99. The negative TCR and $T^{\frac{1}{2}}$ behavior of σ with finite σ_0 suggest a conducting phase analogous to a disordered metal [33,46] for $n \geq 0.89$. Note that deviations from the characteristic metallic behavior obeying the well-known Boltzmann or Bloch-Grüneisen transport are observed in disordered metals, deformable lattices, metallic glasses, and amorphous metals [31,32,47–49]. In disordered systems [33,50] and in deformable lattices [31] in particular, transport immediately above the MIT is characterized by diffusive or extended states.

The n dependence of ρ at 300 K is plotted for $\text{Na}_n/\text{Na}_2\text{-P}$, $\text{K}_n/\text{K}_2\text{-P}$ [15], and $\text{Rb}_n/\text{Rb}_2\text{-P}$ in Fig. 3(b). For $\text{K}_n/\text{K}_2\text{-P}$, a decrease in ρ (300 K) of more than four orders of magnitude

TABLE I. Parameters used to fit the small-polaron absorption spectrum given by Eq. (1) to optical absorptions shown in Figs. 2(c)–(e).

| n | E_b (eV) | E_{vib} (eV) |
|---|-----------------|-----------------------|
| 0.05 ($\text{Na}_n/\text{Na}_2\text{-P}$) | 1.34 ± 0.05 | 0.031 ± 0.004 |
| 0.41 ($\text{Na}_n/\text{Na}_2\text{-P}$) | 1.11 ± 0.06 | 0.037 ± 0.002 |
| 0.12 ($\text{Rb}_n/\text{Rb}_2\text{-P}$) | 0.57 ± 0.02 | 0.038 ± 0.003 |

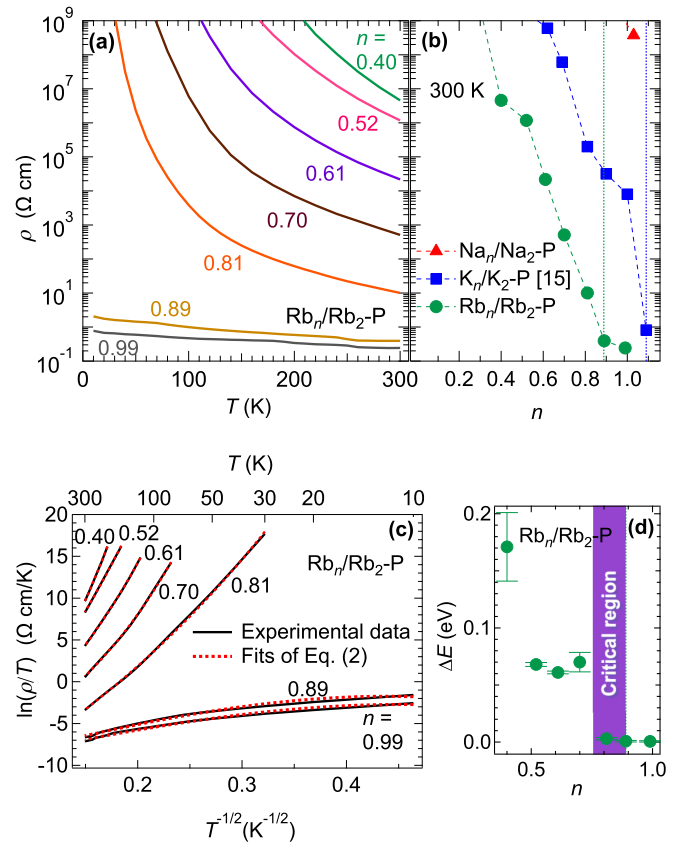


FIG. 3. Transport properties of $\text{Na}_n/\text{Na}_2\text{-P}$, $\text{K}_n/\text{K}_2\text{-P}$, and $\text{Rb}_n/\text{Rb}_2\text{-P}$. (a) The T dependence of ρ pertaining to $\text{Rb}_n/\text{Rb}_2\text{-P}$. (b) The n dependence of ρ at 300 K for $\text{Na}_n/\text{Na}_2\text{-P}$, $\text{K}_n/\text{K}_2\text{-P}$ [15], and $\text{Rb}_n/\text{Rb}_2\text{-P}$. The dashed lines are guides for the eye. The vertical green and blue dotted lines indicate the n at which a conducting phase is observed in $\text{Rb}_n/\text{Rb}_2\text{-P}$ and $\text{K}_n/\text{K}_2\text{-P}$ [15], respectively. (c) Fits of the model given in Eq. (2) for $\text{Rb}_n/\text{Rb}_2\text{-P}$. (d) The n dependence of estimated ΔE for $\text{Rb}_n/\text{Rb}_2\text{-P}$. The shaded area marks a critical region, as explained in the text. The vertical dotted line indicates the conducting phase at $n = 0.89$.

occurs for $n > 1$, which yields an abrupt conducting phase at $n = 1.09$; this behavior suggests a discontinuous transition [15]. For $\text{Rb}_n/\text{Rb}_2\text{-P}$, ρ (300 K) is smaller at comparable values of n . In stark contrast to $\text{K}_n/\text{K}_2\text{-P}$, a crossover to a conducting phase is observed at $n = 0.89$.

The T^{-1} laws characteristic of an activation process [$\rho \propto \exp(E_a/k_B T)$] or adiabatic nearest-neighbor hopping [$\rho \propto T \exp(E_a/k_B T)$], where E_a is the activation energy and k_B is the Boltzmann constant, do not fit our data well. Further, our data cannot be fit to the variable-range-hopping (VRH) model proposed by Mott for noninteracting carriers [51,52], i.e., $\rho \propto \exp(T_0/T)^\nu$, where $\nu = 1/4$ or $1/3$ for a three-dimensional or 2D system, respectively, $T_0 = 24/[\pi k_B N(E_F)\xi^3]$ is a parameter related to the density of localized states at the Fermi level $N(E_F)$, and ξ is the decay length of the localized wave function associated with the charge carriers. Similarly, the VRH model of Efros and Shklovskii (ES-VRH) incorporating electron-electron correlations does not fit our data well. This model is expressed as $\rho \propto \exp(T^*/T)^{\frac{1}{2}}$ [53,54], where $T^* = 2.8e^2/[4\pi\epsilon_0\epsilon k_B\xi]$, ϵ_0 is the permittivity of vacuum, and ϵ is the dielectric constant of the material. In some cases, combinations

TABLE II. Parameters used to fit the T dependence of ρ pertaining to $\text{Rb}_n/\text{Rb}_2\text{-P}$ with the model given in Eq. (2) together with the values of ρ at 300 K.

| n | ΔE (eV) | T^* (K) | ρ ($\Omega\text{ cm}$) |
|------|---------------------|--------------------|-------------------------------|
| 0.40 | 17×10^{-2} | 6.21×10^4 | 4.6×10^6 |
| 0.52 | 68×10^{-3} | 6.99×10^4 | 1.2×10^6 |
| 0.61 | 61×10^{-3} | 4.29×10^4 | 2.2×10^4 |
| 0.70 | 70×10^{-3} | 1.28×10^4 | 5.1×10^2 |
| 0.81 | 3×10^{-3} | 2.60×10^4 | 1.0×10^1 |
| 0.89 | 8×10^{-4} | 2.89×10^3 | 3.9×10^{-1} |
| 0.99 | 6×10^{-4} | 1.83×10^3 | 2.4×10^{-1} |

of the aforementioned models have been used to fit transport data for perovskite-related ceramics, transition-metal oxides, and semiconductor nanocrystal solids [55–59]. However, for simultaneous contributions to σ over the entire T range or separate contributions in different T ranges, such combinations fail to yield consistent fits to our experimental data.

Here, we employ a two-step mechanism [60],

$$\rho = AT \exp \left[\left(\frac{\Delta E}{k_B T} \right) + \left(\frac{T^*}{T} \right)^{\frac{1}{2}} \right], \quad (2)$$

where A is a constant and ΔE is the activation energy required to move to an intermediate state with weakened E_b . The weakly bound intermediate state can hop (ES-VRH [53]) to an appropriate site having a minimum energy difference in the random potential by overcoming the Coulomb interactions. This model yields better fits than the various models described above, and these fits are shown in Fig. 3(c). The fitting parameters are summarized in Table II, and the estimated values of ΔE are plotted in Fig. 3(d). Note that ΔE is almost constant in the range $0.52 \leq n \leq 0.70$, even though ρ at 300 K continues to decrease by four orders of magnitude. At $n = 0.81$, still within the insulating phase, ΔE decreases notably, perhaps indicating the onset of a critical region as discussed later. Finally, ΔE becomes zero (within the error) at $n = 0.89$.

We measured the T dependence of the magnetization and performed Curie-Weiss (CW) analysis of all the samples pertaining to $\text{Na}_n/\text{Na}_2\text{-P}$ and $\text{Rb}_n/\text{Rb}_2\text{-P}$. The T dependence of the magnetic susceptibility χ of $\text{Na}_n/\text{Na}_2\text{-P}$ is shown in Fig. 4(a) for $n = 0.29, 0.41, 0.71, 0.83$, and 1.03 . An increase in χ with increasing T (> 100 K) is apparent for some samples (for instance, $n = 0.41$ and 0.83), rendering it difficult to perform the CW analysis over the entire measured T range. Similar behavior is observed for $\text{Na}_2\text{-P}$, indicating that this behavior is extrinsic to the guest Na atoms. The CW fit for $n = 0.71$ is shown in Fig. 4(c), where χ_0 is a constant balancing the diamagnetic component of the glass tube. At 100% occupancy for a localized spin $S = \frac{1}{2}$ in each cage, the Curie constant C is 2.44×10^{-3} K emu/cm³. A minority ($< 3\%$) of guest electrons carry a magnetic moment of $S = \frac{1}{2}$, and these unpaired states highlight the disorder. The majority of electrons are in a nonmagnetic (paired) state.

The T dependence of χ pertaining to $\text{Rb}_n/\text{Rb}_2\text{-P}$ is shown in Fig. 4(b) for $n = 0.29, 0.52, 0.70, 0.81$, and 0.89 . The CW fit for $n = 0.70$ is shown in Fig. 4(d). The n dependence of

the estimated C is plotted in Fig. 4(e). Similar to $\text{Na}_n/\text{Na}_2\text{-P}$, the majority of guest electrons are in a nonmagnetic state. A sudden drop in C is observed as $\text{Rb}_n/\text{Rb}_2\text{-P}$ enters the conducting phase at $n = 0.89$. The reason for this decrease is unclear.

IV. DISCUSSION

The ground state(s), its stability, and phase transitions of electrons in a deformable lattice remain under debate. Plausible explanations require considerations of the polaron [1–4,10,18,19,61] and electron correlation [62–64] effects. At $n = 0.05$, $\text{Na}_n/\text{Na}_2\text{-P}$ is nonmagnetic and insulating. These features, together with the characteristic polaron absorption band at approximately $21\,000\text{ cm}^{-1}$ [Fig. 2(a)], suggest the formation of small bipolarons with a strong E_b of 1.34 eV [Fig. 2(c)]. We are unable to conclude whether these are intra- [43] or intersite [6]. The growth of the band at approximately $21\,000\text{ cm}^{-1}$ suggests an increase in the number density of small bipolarons [40]. At $n = 0.41$, this band is largely reduced, transferring spectral weight to a new band at approximately $16\,000\text{ cm}^{-1}$ yielding an E_b of 1.11 eV [Fig. 2(d)]. Note that the cage voids of adjacent zigzag channels form a diamond lattice [see Fig. 1(a)], and the percolation threshold for paired constituents in a diamond lattice is 0.35 [65]. The value of n (≈ 0.4) at which the abrupt change occurs coincides with this threshold (hinting at the intersite nature of the small bipolarons). The percolation of small bipolarons generates a new phase, which is likely a polaron Wigner lattice (PWL) [66–68]. The onset of interactions in the many-polaron system may relax the large lattice displacements, weakening E_b . The growth of the band at approximately $16\,000\text{ cm}^{-1}$ with increasing n suggests an increase in the density in the many-polaron system. Despite the increasing interactions, the mobility gap of the stubborn bipolaronic insulator $\text{Na}_n/\text{Na}_2\text{-P}$ remains open. Although some shoulders appear in the absorption tail at high n (≥ 0.83), there are no apparent links to the transport properties.

The $\text{Rb}_n/\text{Rb}_2\text{-P}$ samples also exhibit characteristic polaron absorption at approximately 8500 cm^{-1} [Fig. 2(b)] yielding an E_b of 0.57 eV [Fig. 2(e)]. The nonmagnetic and insulating phase suggests the formation of small bipolarons. We conjecture that the most plausible ground state is intersite [6], forming a paired state despite the weaker λ through reduction of U [69]. The small bipolaron band of $\text{Rb}_n/\text{Rb}_2\text{-P}$ is sharper and at a lower frequency compared to that of $\text{Na}_n/\text{Na}_2\text{-P}$ [Fig. 2(f)]. Smaller Frank-Condon displacements at weaker λ can explain this behavior [40], providing further evidence of the polaronic nature of these bands. The growth of the band at approximately 8500 cm^{-1} suggests an increase in the number density of small bipolarons. At $n = 0.40$, a new band appears at approximately $14\,500\text{ cm}^{-1}$, which coexists with the small bipolaron band [Fig. 2(b)]. This behavior differs from $\text{Na}_n/\text{Na}_2\text{-P}$, where the small bipolaron band exhibits a sudden redshift. (Stronger E_b suggests a comparatively larger lattice displacement that is hence strongly susceptible to the relaxations in the lattice [14].) The onset of interactions in the many-polaron system [65] can result in a photoinduced many-electron effect within the quasi-2D slabs in a weakly localized scenario. The excitations of many electrons in a slab can produce a finite depolarization

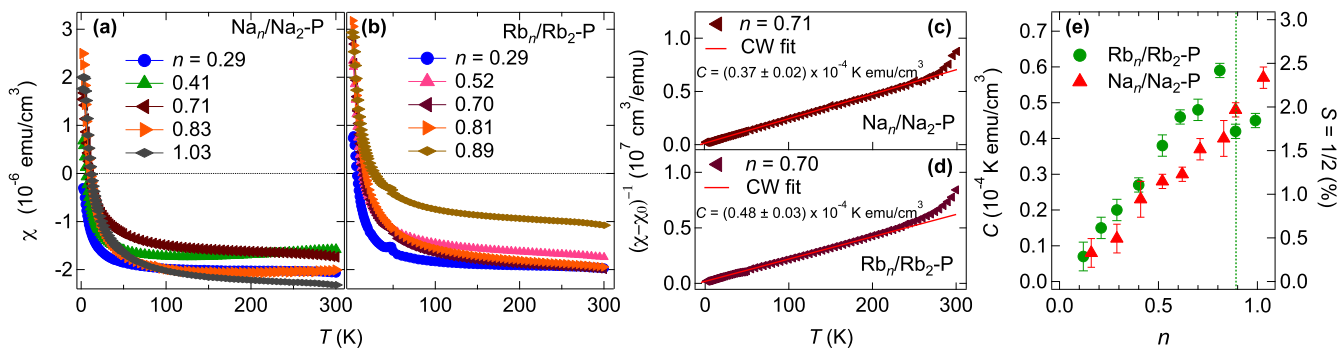


FIG. 4. Magnetic properties of $\text{Na}_n/\text{Na}_2\text{-P}$ and $\text{Rb}_n/\text{Rb}_2\text{-P}$. The T dependence of χ pertaining to (a) $\text{Na}_n/\text{Na}_2\text{-P}$, at $n = 0.29, 0.41, 0.71, 0.83,$ and 1.03 , and (b) $\text{Rb}_n/\text{Rb}_2\text{-P}$, at $n = 0.29, 0.52, 0.70, 0.81,$ and 0.89 . Curie-Weiss fit for (c) $\text{Na}_n/\text{Na}_2\text{-P}$, at $n = 0.71$, and (d) $\text{Rb}_n/\text{Rb}_2\text{-P}$, at $n = 0.70$. (e) The n dependence of estimated C for $\text{Na}_n/\text{Na}_2\text{-P}$ and $\text{Rb}_n/\text{Rb}_2\text{-P}$. The right axis gives the percentage of guest electrons carrying a magnetic moment of spin $S = \frac{1}{2}$. The vertical dotted line indicates the conducting phase of $\text{Rb}_n/\text{Rb}_2\text{-P}$ at $n = 0.89$.

field, inducing the surface-plasmon effect in the polarization parallel to the c axis. For $n = 0.40$, the electron density $n_e \approx 0.32 \times 10^{22} \text{ cm}^{-3}$ (considering the cavity volume [36]). An analogy with the bulk plasmon of Rb [70] gives a surface plasmon energy of 1.81 eV (14600 cm^{-1}), with remarkable agreement with the band at approximately 14500 cm^{-1} for $n = 0.40$. The oscillator strength and the energy of the surface plasmon increase with n_e , in agreement with the observed behavior.

The electron-lattice coupling induces “incoherent” contributions, generating multiphonon absorption bands in the MIR. Such bands are observed in other polaron materials such as V_3O_5 [71], Fe_3O_4 [72], and doped $(\text{SrMnO}_3)_m/(\text{LaMnO}_3)_{2m}$ superlattices [73]. The first MIR band at approximately 3300 cm^{-1} appears at $n = 0.40$ immediately above the percolation threshold [65] [Fig. 2(b)], exactly where ρ at 300 K exhibits a value below the measurement limit in $\text{Rb}_n/\text{Rb}_2\text{-P}$ [Fig. 3(b)]. In this scenario, the MIR band at approximately 3300 cm^{-1} is ascribed to photoinduced hopping of small bipolarons [41,74]. Further, ΔE remains almost constant for $0.52 \leq n \leq 0.70$, despite the decrease in ρ at 300 K by four orders of magnitude. This suggests an increase in the number density of small bipolarons (also indicated by the growth of the band at approximately 8500 cm^{-1}), which equally contribute to σ . The charge transport in the region $0.52 \leq n \leq 0.70$ is ascribed to thermal activation followed by ES-VRH behavior [Eq. (2)] in the random potential of the many-polaron system.

Polarons collapse into a self-trapped state and remain as such or melt and disassociate, depending on the critical balance between E_b and half the bare electronic bandwidth [68,75]. At $n = 0.81$, $\text{Rb}_n/\text{Rb}_2\text{-P}$ enters (or is already within) a critical region, where the increasing density (likely in a PWL) induces continuous melting [68] of small bipolarons, indicated by the reduction in the band at 8500 cm^{-1} [Fig. 2(b)] and the drop in ΔE [Fig. 3(d)]. At $n = 0.89$, as $\text{Rb}_n/\text{Rb}_2\text{-P}$ enters a conducting phase, a second MIR band appears at approximately 2500 cm^{-1} , simultaneous with the closing of ΔE . The estimated T^* exhibits a decrease of one order of magnitude in the conducting phase (Table II). Assuming that ε remains constant across the crossover, ξ exhibits an increase

of one order of magnitude, indicating the extended nature of the charge transport [32,33,44]. The appearance of the second MIR band perhaps signals the incoherent polaronic nature of the transport in the conducting phase [71–73], likely a large polaron with short-range electron-lattice coupling [40]. The phase diagram of the continuous transition from localized to critical to extended states of $\text{Rb}_n/\text{Rb}_2\text{-P}$ is shown in Fig. 5. The transition from extended states to characteristic metallic behavior is perhaps triggered at a considerably weaker λ . The coexistence of the small bipolaron (although reduced) and the MIR bands suggests a degenerate polaron liquid [76]. In this scenario, a two-fluid model of extended states and thermally activated carriers of localized states [77] seems appropriate for explaining the negative TCR, which remains puzzling above the MIT of disordered metals [31,33].

In summary, the electronic properties of guest Na ($\text{Na}_n/\text{Na}_2\text{-P}$) and Rb atoms ($\text{Rb}_n/\text{Rb}_2\text{-P}$) in a disordered deformable lattice were investigated at various guest-atom densities n using optical, magnetic, and transport measurements. $\text{Na}_n/\text{Na}_2\text{-P}$ is a stubborn bipolaronic insulator. $\text{Rb}_n/\text{Rb}_2\text{-P}$ undergoes a crossover from small bipolarons to a conducting phase analogous to a disordered metal. Opening of a mobility gap at strong λ and the continuous conducting transition at comparatively weak λ reflect the recent theory that discusses electron-lattice coupling and Anderson localization on the same footing [31]. This is in disagreement with

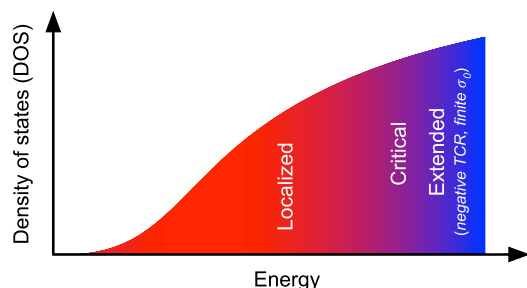


FIG. 5. Phase diagram of $\text{Rb}_n/\text{Rb}_2\text{-P}$ depicting a continuous transition from localized to critical to extended states.

the suggested discontinuous transition [29,30]. However, we conjecture the presence of a narrow region of λ for which the discontinuity holds true, where the K counterpart fits in [15]. Electron-lattice coupling can freeze or trigger a conducting transition and scale its continuity (or discontinuity) as a result of the nontrivial interplay of disorder and the correlated response of a deformable lattice to the random potential. Investigations in this direction have the potential to explain many puzzling properties of disordered metals near the metal-insulator transition and to solve the conundrum of Mooji correlations.

ACKNOWLEDGMENTS

G.P.H. thanks S. Tamiya for performing the chemical analyses and Y. Nozue for providing the starting material and experimental facilities. G.P.H. is indebted to M. S. Osofsky for fruitful discussions and assistance with the direction of this manuscript. G.P.H. acknowledges support from the Research Promotion Division of Osaka University and the Ministry of Education, Culture, Sports, Science and Technology of Japan under the program for promoting research activities and enhancement of research universities.

-
- [1] L. D. Landau, *Phys. Z. Sowjetunion* **3**, 664 (1933); *Collected Papers* (Gordon and Breach, New York, 1965) [English translation].
- [2] S. I. Pekar, *Research in Electron Theory of Crystals* (Gostekhizdat, Moscow, 1951); *Research in Electron Theory of Crystals*, US AEC Report No. AEC-tr-5575 US Atomic Energy Commission, Oak Ridge, TN, (1963) [English translation].
- [3] H. Fröhlich, *Adv. Phys.* **3**, 325 (1954).
- [4] D. Emin, *Polarons* (Cambridge University Press, Cambridge, 2013).
- [5] A. Bussmann-Holder and H. Keller, *J. Supercond. Nov. Magn.* **22**, 123 (2009).
- [6] *Polarons in Advanced Materials*, edited by A. S. Alexandrov (Springer, Dordrecht, 2007).
- [7] *Semimagnetic Semiconductors and Diluted Magnetic Semiconductors*, edited by M. Averous and M. Balkanski (Springer, New York, 1991).
- [8] X. Liu, M. Wiemer, A. V. Nenashev, S. Petznick, P. J. Klar, M. Hetterich, F. Gebhard, and S. D. Baranovskii, *J. Appl. Phys.* **116**, 083710 (2014).
- [9] A. J. Millis, *Nature (London)* **392**, 147 (1998).
- [10] T. Nakano and Y. Nozue, *Adv. Phys. X* **2**, 254 (2017).
- [11] J. Kim, A. N. Unterreiner, S. Rane, S. Park, J. Jureller, L. Book, Y. H. Liao, and N. F. Scherer, *J. Phys. Chem. B* **106**, 12866 (2002).
- [12] E. Romero, R. Augulis, V. I. Novoderezhkin, M. Ferretti, J. Thieme, D. Zigmantas, and R. van Grondelle, *Nat. Phys.* **10**, 676 (2014).
- [13] A. J. E. Rettie, W. D. Chemelewski, D. Emin, and C. B. Mullins, *J. Phys. Chem. Lett.* **7**, 471 (2016).
- [14] Y. Nozue, Y. Amako, R. Kawano, T. Mizukane, and T. Nakano, *J. Phys. Chem. Solids* **73**, 1538 (2012).
- [15] G. P. Hettiarachchi, T. Nakano, Y. Masaki, M. N. M. Muhid, H. Hamdon, and Y. Nozue, *J. Phys. Soc. Jpn.* **84**, 014702 (2015).
- [16] L. Yu, *Solitons and Polarons in Conducting Polymers* (World Scientific, Singapore, 1988).
- [17] X. Liu, K. Gao, Y. Li, J. Fu, J. Wei, and S. Xie, *Synth. Met.* **157**, 380 (2007).
- [18] I. G. Austin and N. F. Mott, *Adv. Phys.* **18**, 41 (1969).
- [19] T. Holstein, *Ann. Phys. (NY)* **8**, 343 (1959).
- [20] A. N. Jette, T. L. Gilbert, and T. P. Das, *Phys. Rev.* **184**, 884 (1969).
- [21] T. D. Lee, F. E. Low, and D. Pines, *Phys. Rev.* **90**, 297 (1953).
- [22] D. Emin, *Comments Solid State Phys.* **11**, 35 (1983).
- [23] E. Abrahams, P. W. Anderson, D. C. Licciardello, and T. V. Ramakrishnan, *Phys. Rev. Lett.* **42**, 673 (1979).
- [24] W. L. McMillan, *Phys. Rev. B* **24**, 2739 (1981).
- [25] P. W. Anderson, *Phys. Rev.* **109**, 1492 (1958).
- [26] M. Osofsky, H. Tardy, M. LaMadrid, and J. M. Mochel, *Phys. Rev. B* **31**, 4715 (1985).
- [27] G. Hertel, D. J. Bishop, E. G. Spencer, J. M. Rowell, and R. C. Dynes, *Phys. Rev. Lett.* **50**, 743 (1983).
- [28] D. Emin and T. Holstein, *Phys. Rev. Lett.* **36**, 323 (1976).
- [29] M. H. Cohen, E. N. Economou, and C. M. Soukoulis, *Phys. Rev. Lett.* **51**, 1202 (1983).
- [30] M. H. Cohen, E. N. Economou, and C. M. Soukoulis, *Phys. Rev. B* **29**, 4500 (1984).
- [31] D. Di Sante, S. Fratini, V. Dobrosavljević, and S. Ciuchi, *Phys. Rev. Lett.* **118**, 036602 (2017).
- [32] P. A. Lee and T. V. Ramakrishnan, *Rev. Mod. Phys.* **57**, 287 (1985).
- [33] M. S. Osofsky, C. M. Krowne, K. M. Charipar, K. Bussmann, C. N. Chervin, I. R. Pala, and D. R. Rolison, *Sci. Rep.* **6**, 21836 (2016).
- [34] H. Hamdan, M. N. M. Muhid, S. Endud, E. Listiorini, and Z. Ramli, *J. Non-Cryst. Solids* **211**, 126 (1997).
- [35] W. Loewenstein, *Am. Mineral.* **39**, 92 (1954).
- [36] G. Vezzalini, A. Sani, and M. Triscari, *Microporous Mesoporous Mater.* **31**, 253 (1999).
- [37] P. Kubelka and F. Munk, *Z. Tech. Phys.* **12**, 593 (1931).
- [38] J. Texter, D. H. Strome, R. G. Herman, and K. Klier, *J. Phys. Chem.* **81**, 333 (1977).
- [39] H. G. Reik and D. Heese, *J. Phys. Chem. Solids* **28**, 581 (1967).
- [40] D. Emin, *Phys. Rev. B* **48**, 13691 (1993).
- [41] M. I. Klinger, *Phys. Lett.* **7**, 102 (1963).
- [42] P. Calvani, *Riv. Nuovo Cimento Soc. Ital. Fis.* **8**, 1 (2001).
- [43] N. F. Mott, *Metal-Insulator Transitions* (Taylor and Francis, London, 1990).
- [44] N. Nishida, M. Yamaguchi, T. Furubayashi, K. Morigaki, H. Ishimoto, and K. Ono, *Solid State Commun.* **44**, 305 (1982).
- [45] A. L. Efros and M. Pollak, *Electron-Electron Interactions in Disordered Systems* (North-Holland, Amsterdam, 1985).
- [46] C. O. Yoon, Reghu M., D. Moses, and A. J. Heeger, *Phys. Rev. B* **49**, 10851 (1994).
- [47] B. W. Dodson, W. L. McMillan, J. M. Mochel, and R. C. Dynes, *Phys. Rev. Lett.* **46**, 46 (1981).
- [48] W. L. McMillan and J. Mochel, *Phys. Rev. Lett.* **46**, 556 (1981).
- [49] D. Belitz and T. R. Kirkpatrick, *Rev. Mod. Phys.* **66**, 261 (1994).
- [50] T. F. Rosenbaum, R. F. Milligan, M. A. Paalanen, G. A. Thomas, R. N. Bhatt, and W. Lin, *Phys. Rev. B* **27**, 7509 (1983).
- [51] N. F. Mott, *J. Non-Cryst. Solids* **1**, 1 (1968).

- [52] N. F. Mott and E. A. Davis, *Electronic Processes in Non-Crystalline Materials* (Clarendon, Oxford, 1979).
- [53] A. L. Efros and B. I. Shklovskii, *J. Phys. C* **8**, L49 (1975).
- [54] D. N. Tsigankov and A. L. Efros, *Phys. Rev. Lett.* **88**, 176602 (2002).
- [55] L. Zhang and Z. J. Tang, *Phys. Rev. B* **70**, 174306 (2004).
- [56] K. Maiti, N. Y. Vasanthacharya, and D. D. Sarma, *J. Phys. Condens. Matter* **9**, 7507 (1997).
- [57] M. H. Sage, G. R. Blake, and T. T. M. Palstra, *Phys. Rev. B* **77**, 155121 (2008).
- [58] D. Yu, C. Wang, B. L. Wehrenberg, and P. Guyot-Sionnest, *Phys. Rev. Lett.* **92**, 216802 (2004).
- [59] I. Ahmad, M. J. Akhtar, R. T. A. Khan, and M. M. Hasan, *J. Appl. Phys.* **114**, 034103 (2013).
- [60] Y. Sun, X. Xu, and Y. Zhang, *J. Phys. Condens. Matter* **12**, 10475 (2000).
- [61] Y. Toyozawa, *Prog. Theor. Phys.* **26**, 29 (1961).
- [62] B. K. Chakraverty, *Nature (London)* **287**, 393 (1980).
- [63] R. Arita, T. Miyake, T. Kotani, M. van Schilfgarde, T. Oka, K. Kuroki, Y. Nozue, and H. Aoki, *Phys. Rev. B* **69**, 195106 (2004).
- [64] K. Nakamura, T. Koretsune, and R. Arita, *Phys. Rev. B* **80**, 174420 (2009).
- [65] H. Holloway, *Phys. Rev. B* **37**, 874 (1988).
- [66] E. P. Wigner, *Phys. Rev.* **46**, 1002 (1934).
- [67] C. C. Grimes and G. Adams, *Phys. Rev. Lett.* **42**, 795 (1979).
- [68] Z. Lenac and M. Šunjić, *Phys. Rev. B* **59**, 6752 (1999).
- [69] M. H. Cohen, E. N. Economou, and C. M. Soukoulis, *Phys. Rev. B* **29**, 4496 (1984).
- [70] B. M. Hartley and J. B. Swan, *Phys. Rev.* **144**, 295 (1966).
- [71] L. Baldassarre, A. Perucchi, E. Arcangeletti, D. Nicoletti, D. Di Castro, P. Postorino, V. A. Sidorov, and S. Lupi, *Phys. Rev. B* **75**, 245108 (2007).
- [72] L. V. Gasparov, D. B. Tanner, D. B. Romero, H. Berger, G. Margaritondo, and L. Forro, *Phys. Rev. B* **62**, 7939 (2000).
- [73] A. Perucchi, L. Baldassarre, A. Nucara, P. Calvani, C. Adamo, D. G. Schlom, P. Orgiani, L. Maritato, and S. Lupi, *Nano Lett.* **10**, 4819 (2010).
- [74] D. Emin, *Adv. Phys.* **24**, 305 (1975).
- [75] H. De Raedt and A. Lagendijk, *Phys. Rev. B* **27**, 6097 (1983).
- [76] S. Fratini and P. Quémerais, *Eur. Phys. J. B* **14**, 99 (2000).
- [77] V. V. Kabanov and D. K. Ray, *Phys. Rev. B* **52**, 13021 (1995).